An index based on fracture length and aperture to predict groundwater inflow rates in tunnels excavated in fractured-rock

Alireza Shahbazi[1*], Ali Saeidi[1], Romain Chesnaux[1], Alain Rouleau[1]

[1]Université du Québec à Chicoutimi, 555 boulevard de l'Université, Chicoutimi, Québec G7H 2B1, Canada

*Alireza Shahbazi: ashahbazi@etu.uqac.ca , orcid: 0000-0001-9595-8948

Ali Saeidi: ali_saeidi@uqac.ca, orcid: 0000-0001-6954-5453

Romain Chesnaux: romain_chesnaux@uqac.ca, orcid: 0000-0002-1722-9499

Alain Rouleau: alain_rouleau@uqac.ca, orcid : 0000-0003-1012-9898

Highlights

- An index has been developed to predict and classify the inflow rate to the tunnel
- The inflow rate to the tunnel increases with the increase of the inflow index
- Inflow index varies by joint characteristics, tunnel radius and the joint orientation
- The prediction of the inflow rate to the tunnel is validated by analytical method

Abstract

The surface area of the fractures at the wall of a tunnel is used to develop a representative index, as inflow index, for the prediction and the classification of the inflow rate to a tunnel that is excavated in a fractured rock mass. For this purpose, an analytical model has been developed for the calculation of the inflow index based on geometrical characteristics of the discontinuities and of the tunnel. The result of the analytical model is validated by numerical simulations using 3DEC

version 7.0 software. Furthermore, the simulation results demonstrate the capacity of the inflow index to predict the inflow rate to the tunnel. At a constant value of the water head, the inflow rate to the tunnel increases with increasing value of the inflow index. In addition, the inflow rate could be classified to various levels, based on the values of inflow index. The study has identified that the hydraulic aperture, joint spacing, tunnel radius and the angle between tunnel and normal to joint sets have the most important impacts on the inflow index and among them, the effect of hydraulic aperture is the most important one.

Keywords

Inflow index, inflow rate, tunnel, fractured rock mass

1 Introduction

Pre-evaluating the safety of underground structures involves predicting the probability of rock falls from the tunnel wall (Shadabfar, Mahsuli et al. 2022), and also, pre-assessment of expected water seepage into the tunnel (Farhadian, Hassani et al. 2017). Groundwater inflow to a tunnel may deteriorate the mechanical properties of the fractured rock mass, decelerate the tunnel excavation rate (Frenelus, Peng et al. 2021), reduce the availability of water for other users and require efforts for water pumping and treatment, and assessment of the environmental impact on water resources (Lv, Jiang et al. 2020). Underground tunnels are mostly excavated in a hard rock formation, that can almost be considered as an impermeable formation. On the other hand, rock mass includes at least one family of joint sets and hence, the fractures are considered as the main route for transferring water into the tunnel (Herbert, Gale et al. 1991). Furthermore, minimum required mechanical characteristics of the rock mass for being certain about the stability of the underground excavations, necessitates that the tunnel being excavated in a rock with maximum mechanical strength, e.g., crystalline rocks (Hudson, Cosgrove et al. 2011, Frenelus, Peng et al. 2021). However,

the permeability of the matrix of these types of rocks is quite low and can often be considered as an impermeable (Shahbazi, Saeidi et al. 2020). In most cases however the presence of fractures constitute the sole conduit for transferring groundwater into underground tunnel (Shahbazi, Chesnaux et al. 2021, Shahbazi, Saeidi et al. 2021, Shahbazi, Saeidi et al. 2023).

Based on Darcy's law (Darcy 1856), the surface area perpendicular to the flow direction is an important parameter that affects the amount of flow. In the case of flow through a fracture, the surface area of the fracture aperture in the plane perpendicular to flow is the effective surface area of flow; hence, the quantification of this parameter is important for estimating the flow rate. On the other hand, the permeability of the fractures is directly related to the hydraulic aperture and on this basis, the total flow rate could be formulated in relation to the hydraulic aperture and length of the fractures. From now on, this formulation is named as the inflow index. For the case of excavation of a tunnel in a fractured rock mass, the inflow index could be determined by knowing the total length of the fractures at the wall of the tunnel. Determination of the inflow index and its relation to the inflow rate to the tunnel is the subject of this article. For this purpose, the analytical method has been applied for determination of the inflow index and is validated by numerical simulation using 3DEC version 7.0 software.

To illustrate the importance of the inflow index on the inflow rate to the tunnel, a series of numerical simulations has been performed. For this purpose, a circular tunnel with a fixed radius is excavated in a fractured rock mass that includes at least one joint set, and a fixed water level (head) above the tunnel is applied on the numerical models. Finally, by numerically determined inflow rate and inflow index as well as analytically determined inflow index, the relationship between inflow rate and inflow index has been discussed.

2 Methodology

To create an analytical model for defining the inflow index, we assume that the rock mass includes at least one joint set. All the fractures are fully persistent, and the geometrical characteristics of the joint sets are fixed, i.e., constant values of aperture, spacing and orientation. A circular tunnel, with a specified diameter, is assumed to be excavated within the rock mass with a predetermined orientation. Furthermore, it is crucial to emphasize that the analytical method presented in this work is tailored for application to unsupported tunnels exclusively and does not encompass supported tunnel structures. Configurations involving reinforcement through structural support systems like bolts, arches, or linings are outside the scope of this analytical model. By considering these assumptions as well as knowing the orientation of the tunnel and joint sets, the trace length of the joints at the wall of the tunnel can be identified and then, the inflow index can be computed by multiplying the trace length by hydraulic aperture. In Section 2.1, the analytical model for defining the inflow index is developed and then validated in section 2.2 by the numerical simulation using 3DEC version 7 software. Finally, in section 2.3, the relationship between inflow index and inflow rate to the tunnel is presented.

2.1 Analytical model for inflow index

Based on Darcy's law (Darcy 1856), the flow rate through a formation could be calculated using Eq.(1).

$$q = -K\, i\, A \qquad (1)$$

Where q is the flow rate (m^3/s), K is the hydraulic conductivity (m/s), i is the hydraulic gradient (m/m) and A is the surface area perpendicular to the flow direction. On the other hand, the cubic law (Witherspoon, Wang et al. 1979) explains the flow of the fluid through parallel plates and could be considered for the case of fluid flow via the fractures, as Eq.(2).

$$K = \frac{\rho g b^2}{12\mu} \quad (2)$$

Where K is the hydraulic conductivity of the fracture (m/s), b is the fracture aperture (m), μ is the dynamic viscosity of the water (kg/m.s), ρ is the fluid density (kg/m^3) and g is the acceleration of gravity (m/s^2). The hydraulic conductivity of fracture is a measure of its ability to transmit fluid, indicating how easily water or other fluids can flow through the fracture, dynamic is a measure of its internal resistance to flow under shear stress, expressed in units of Pascal-seconds (Pa·s). In addition, the surface area perpendicular to the flow direction for the case of inflow into the tunnel through the fracture aperture, could be determined using Eq.(3).

$$A = P \times b \quad (3)$$

Where P is the trace length of the fractures at the wall of the tunnel (m). By substituting A from Eq.(3) and K from Eq.(2) into Eq.(1), the inflow rate could be calculated by Eq.(4).

$$q = -\frac{\rho g b^2}{12\mu} . i . (P \times b) = \frac{\rho g}{12\mu} . i . (P \times b^3) \quad (4)$$

For the case that the rock mass includes more than one joint set, Eq.(4) changes to Eq.(5) for calculation of the average inflow rate per unit length of the tunnel (q_{avg}).

$$q_{avg} = -\frac{\rho g}{12\mu} . i . \sum_i \sum_j (f_i^* \times P_i \times b_{ij}^3) \quad (5)$$

Where index ij denotes the j^{th} fracture of i^{th} joint set, and f^*_i is the apparent frequency of the joint set i at the wall of the tunnel (m^{-1}). As density, viscosity and gravitational acceleration are constant values and the hydraulic gradient at the wall of the tunnel mostly depends on the water head above the tunnel, the last part of Eq.(5) is considered as the *inflow index* in this article, according to Eq.(6).

$$inflow\ index = \sum_i \sum_j (f_i^* \times P_i \times b_{ij}^3) \qquad (6)$$

To determine the *inflow index*, one must ascertain the trace length of each fracture, as well as the apparent frequency of the joint sets at the wall of the tunnel. If the cross section of the tunnel is a circle with radius of R and j^{th} fracture of i^{th} joint set being considered, the trace of the fracture at the wall of the tunnel will be a circle in perpendicular intersection and an ellipse, in oblique intersection of joint set and tunnel, as depicted in Fig 1.

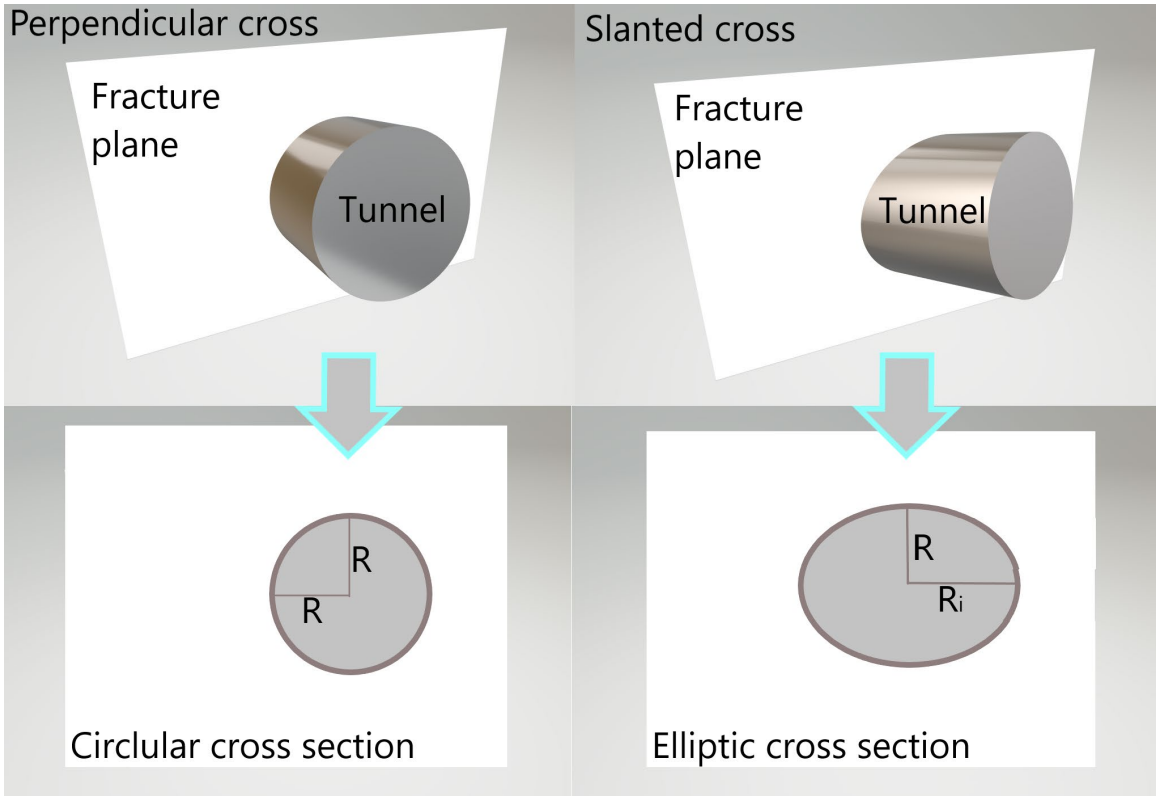

Fig 1. Possible probability of the intersection of a plane (fracture) and a cylinder (Tunnel) for a persistent fracture

In Eq.(6), P_i is the perimeter of the circle or ellipse of Fig 1. For a single fracture, P_i could be calculated by Eq.(7).

$$P_i = 2\pi \sqrt{\frac{R^2 + R_i^2}{2}} \qquad (7)$$

Where R is the tunnel radius (m) and R_i is the larger radius of the ellipse, as of Fig 1. On the other hand, R_i could be calculated by knowing the angle between joint set and tunnel, according to Eq.(8)

$$R_i = R \times \frac{1}{cos\,\theta_i} \qquad (8)$$

Where θ_i is the angle between the tunnel direction and normal to joint set i (n_i), as illustrated in Fig 2.

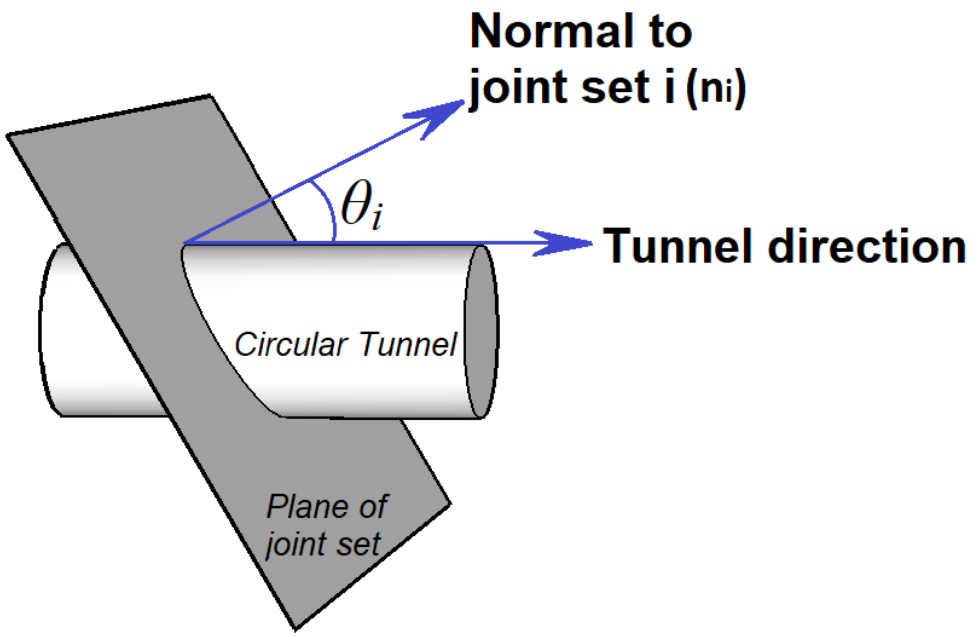

Fig 2. Graphical presentation of the angle between tunnel direction and normal to the joint set i (θ_i)

However, based on the state of the intersection (angle θ_i), the apparent frequency of the i^{th} set (f^*_i) at the wall of the tunnel might be smaller or equal to the real frequency (f_i) of the joint sets. As the frequency is the inverse of spacing ($f_i = 1/S_i$) and by considering Fig 3, f^*_i could be determined using Eq.(9).

$$f_i^* = f_i \times cos\,\theta_i \qquad (9)$$

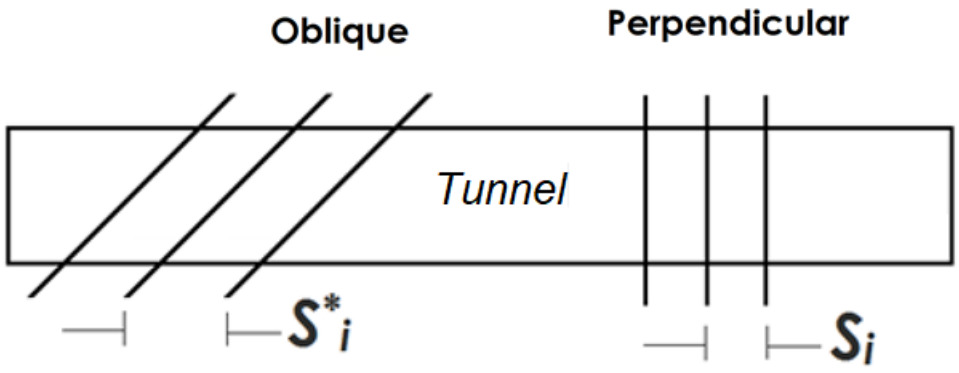

Fig 3. Apparent and real spacing (inverse of frequency) of the joint set i at the wall of the tunnel in the oblique (left hand) and perpendicular (right hand) intersection of joint set and tunnel

As a result, Eq.(9) changes to Eq.(10) if the apparent and true frequencies being substituted by the apparent and true spacings of the joint sets at the wall of the tunnel.

$$S_i^* = \frac{S_i}{cos\,\theta_i} \qquad (10)$$

Where the S_i and S^*_i are the true and apparent spacing of joint sets at the wall of the tunnel, as illustrated in Fig 3. Finally, by combining equations (7)-(10) with Eq. (6), the inflow index could be determined by Eq. (11).

$$inflow\ index = \sum_i \sum_j \frac{2\pi R}{S_i} \sqrt{\frac{1 + cos\,\theta_i}{2}} \times b_{ij}^3 \qquad (11)$$

Inflow index according to Eq.(11) points to the effective area for flow in every meter length of the tunnel with the dimension of L^3 (m^3). In section 2.2, the analytical calculation of the inflow index with Eq. (11) is validated by numerical simulation method using 3DEC software.

2.2 Validation of the analytical method for inflow index

To validate the analytical method for calculation of the inflow index using Eq. (11), Itasca 3DEC version 7 software has been used. For this purpose, twenty cases of the models where a circular tunnel is excavated in a fractured rock mass, are considered, as listed in Table 1. The tunnel has different radius, and the rock mass includes three persistent joint sets. In Table 1, dip refers to the inclination or slope of a joint set in a rock, measured relative to the horizontal plane, and aperture typically refers to the opening or gap between adjacent surfaces or fractures in a rock mass.

Table 1. Comparison of the analytical (Eq.(11)) and numerical modeling (3DEC) results for calculation of the inflow index for twenty cases of rock mass having three persistent joint sets and various radius of the tunnel. JS and DD denote joint set and dip direction, respectively.

	JS1				JS2				JS3				Tunnel	Inflow	Inflow
	Dip	DD	Spacing (m)	Aperture (m)	Dip	DD	Spacing (m)	Aperture (m)	Dip	DD	Spacing (m)	Aperture (m)	Radius (m)	index (m^3) (Eq.(11)	index (m^3) (3DEC)
1	20	20	1	3.00E-03	40	100	2	4.00E-04	70	300	3	1.00E-03	2	2.79E-07	2.73E-07
2	8	259	1	1.82E-04	87	294	3	1.71E-04	3	230	1	4.08E-03	4	1.19E-06	1.19E-06
3	24	121	1	2.20E-05	49	225	2	7.10E-04	35	260	1	3.68E-04	3	2.26E-09	2.28E-09
4	42	186	3	3.93E-04	6	144	1	1.91E-04	38	138	3	4.00E-05	1	8.14E-11	8.09E-11
5	78	1	3	1.00E-05	83	41	2	2.69E-04	24	27	3	4.92E-04	2	5.25E-10	5.20E-10
6	80	171	2	4.19E-04	45	75	4	7.12E-04	46	19	1	1.19E-04	4	1.89E-09	1.92E-09
7	52	184	3	7.55E-04	28	342	2	5.91E-04	35	358	1	9.41E-04	3	1.64E-08	1.68E-08
8	53	307	2	7.20E-04	49	283	4	3.34E-04	90	7	2	9.21E-04	1	3.51E-09	3.44E-09
9	10	166	2	9.74E-04	34	153	2	6.82E-04	53	267	2	3.59E-04	3	7.41E-09	7.48E-09
10	77	171	1	5.86E-04	79	73	4	9.90E-05	9	220	2	3.70E-04	1	2.85E-10	2.71E-10
11	11	4	3	1.98E-04	6	43	2	8.40E-05	30	68	2	9.60E-05	3	4.81E-11	4.81E-11
12	5	52	3	6.38E-04	24	94	4	6.70E-05	5	262	1	7.39E-04	2	4.35E-09	4.37E-09
13	12	203	2	5.77E-04	57	223	1	2.49E-04	49	55	4	1.74E-04	2	8.67E-10	8.78E-10
14	85	119	3	9.46E-04	5	256	3	6.76E-04	66	193	1	8.21E-04	1	2.17E-09	2.22E-09
15	71	230	3	4.81E-04	14	22	2	2.31E-04	37	298	3	4.85E-04	4	1.29E-09	1.40E-09

16	29	249	1	6.84E-04	71	113	4	1.95E-04	26	122	3	9.92E-04	2	5.14E-09	5.18E-09
17	74	215	1	3.81E-04	79	251	1	5.72E-04	59	248	2	8.79E-04	2	4.08E-09	4.01E-09
18	82	226	3	3.91E-04	47	229	3	2.01E-04	48	211	2	5.39E-04	2	5.33E-10	5.22E-10
19	37	132	2	7.00E-04	8	195	1	2.74E-04	20	62	4	7.15E-04	3	3.33E-09	3.33E-09
20	33	50	1	7.07E-04	32	50	1	2.06E-04	88	240	1	4.53E-04	2	4.32E-09	4.23E-09

To calculate the inflow index by numerical method, a FISH function has been embedded in the command lines of the 3DEC software. For this purpose, the trace length of each fracture plane (flow plane) at the wall of the tunnel is separately calculated and multiplied by the cube of the pertinent hydraulic aperture. The applied numerical method for inflow index calculation is schematically illustrated in Fig 4.

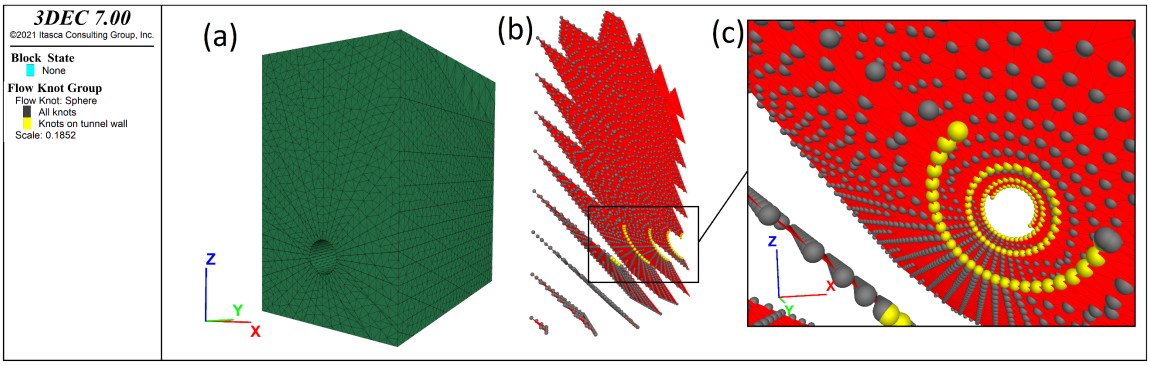

Fig 4. Numerical method for calculation of the inflow index. (a) A numerical model of the rock mass including a joint set. (b) Cross section of the numerical model at the centerline of the tunnel illustrating the flowplanes and flow knots. (c) Larger view of the flowplanes showing the flowknots (yellow spheres) that are common between flow planes and the wall of the tunnel

In Fig 4, the flowplane is the planar polygon corresponding to face-to-face contact between solid blocks, the flowplane zone is a triangular discretization element of the flow plane, and the flowknot is the vertices of a flowplane zone that generally corresponds to a sub-contact between solid blocks (Itasca Consulting Group 2021). In Fig 4c, the yellow flowknots, that coexist in flowplanes and wall of the tunnel, are identified and used for calculation of the trace length of each flowplane

158 (fracture) at the wall of the tunnel. By categorizing the yellow flowknots that belong to one
159 flowplane and defining the coordinates of each of them, the total trace length of a joint set at the
160 wall of the tunnel could be calculated. Finally, by multiplying the trace length of joint set with cube
161 of pertinent hydraulic aperture, the inflow index could be numerically calculated.

162 ## 2.3 Inflow rate and inflow index relationship

163 As discussed in section 2.1 and based on Eq.(11), it becomes evident that the inflow index has a
164 significant impact on the inflow rate to the tunnel and could be calculated by analytical method
165 using Eq.(11) for a tunnel that is excavated in a fractured rock mass that includes persistent joint
166 sets. To validate this effect, a series of numerical simulation with 3DEC version 7 software has
167 been designed according to Table 2, for studying the variation of the inflow rate by inflow index.
168 The numerical simulations comprise of calculating the inflow rate to the tunnel that is excavated in
169 a fractured rock mass for three levels of water head including 10, 40 and 100 meters and three
170 levels of tunnel radius as 1, 2 and 4 meters.

171

Table 2. Geometrical characteristics of the discontinuities and tunnel for evaluation of the relationship between inflow rate to the tunnel and the inflow index. For this purpose, three levels of water head including 10, 40 and 100 meters and three levels of tunnel radius as 1, 2 and 4 meters has been considered for numerical modeling.

	Joint set 1				Joint set 2				Joint set 3				W_h (m)	R (m)	Inflow index (m^3)	Inflow rate ($(m^3/s)/m$)
	Dip (º)	DD (º)	Aperture (m)	Spacing (m)	Dip (º)	DD (º)	Aperture (m)	Spacing (m)	Dip (º)	DD (º)	Aperture (m)	Spacing (m)				
1	90.00	10	0.002	3.94	67.16	340	0.002	0.35	90.00	350	0.0005	3.94	10	1	1.53203E-07	0.489615
2	43.16	60	0.002	0.34	60.00	0	0.002	3.46	23.26	330	0.0005	0.14	10	1	1.39027E-07	0.252559
3	90.00	10	0.00005	0.39	90.00	350	0.00005	0.39	43.16	60	0.002	0.14	10	1	3.00747E-07	0.597561
4	67.16	20	0.00005	0.87	43.16	60	0.00005	1.37	90.00	350	0.00005	0.39	10	1	3.33063E-12	0.000013946
5	43.16	60	0.0005	0.34	61.57	10	0.0005	0.87	67.16	340	0.00005	0.87	10	1	2.75745E-09	0.00568132
6	90.00	30	0.002	3.46	21.34	340	0.00005	0.14	80.00	0	0.002	0.39	10	1	1.40998E-07	0.369845
7	43.16	60	0.002	1.37	80.00	0	0.00005	0.39	21.34	340	0.00005	1.37	10	1	3.00768E-08	0.0517309
8	90.00	30	0.0005	0.87	43.16	60	0.002	0.34	32.15	310	0.002	1.37	10	1	1.51248E-07	0.405854
9	67.16	20	0.002	0.87	80.00	0	0.002	0.39	67.16	340	0.002	0.87	10	1	2.3921E-07	0.518672
10	67.16	20	0.00005	0.35	90.00	70	0.002	0.14	90.00	350	0.00005	3.94	10	1	3.00745E-07	0.57682
11	67.16	20	0.00005	0.87	90.00	70	0.002	0.14	21.34	340	0.0005	0.34	10	2	6.05247E-07	1.38471
12	90.00	350	0.00005	0.98	90.00	10	0.0005	0.98	43.16	60	0.0005	1.37	10	2	2.52844E-09	0.00472948
13	90.00	10	0.002	0.39	90.00	350	0.0005	3.94	90.00	30	0.0005	0.87	10	2	2.56076E-07	0.533161
14	90.00	10	0.002	3.94	90.00	350	0.00005	0.98	90.00	30	0.002	3.46	10	2	5.34559E-08	0.0555941
15	26.52	40	0.00005	1.37	43.16	300	0.002	1.37	80.00	0	0.002	3.94	10	2	8.55421E-08	0.0995077
…	…	…	…	…	…	…	…	…	…	…	…	…	…	…	…	…

78	43.16	60	0.002	0.14	80.00	0	0.002	0.39	67.16	340	0.0005	0.35	100	4	1.71959E-06	40.9046
79	43.16	60	0.00005	1.37	90.00	10	0.0005	3.94	67.16	340	0.00005	0.35	100	4	8.04166E-10	0.00167632
80	90.00	10	0.00005	3.94	90.00	350	0.00005	3.94	80.00	0	0.002	0.98	100	4	2.03142E-07	2.58731
81	90.00	30	0.002	0.35	90.00	350	0.0005	3.94	43.16	60	0.002	1.37	100	4	6.82326E-07	7.40678
82	43.16	60	0.002	1.37	90.00	290	0.00005	0.34	20.00	0	0.002	1.37	100	4	2.40602E-07	3.61091
83	90.00	10	0.00005	0.98	90.00	70	0.002	1.37	43.16	300	0.002	0.14	100	4	1.32327E-06	31.6968

174

The inflow rate and pertinent inflow index that are listed in Table 2, were categorized in three levels of water head above the tunnel and are shown in Fig 5.

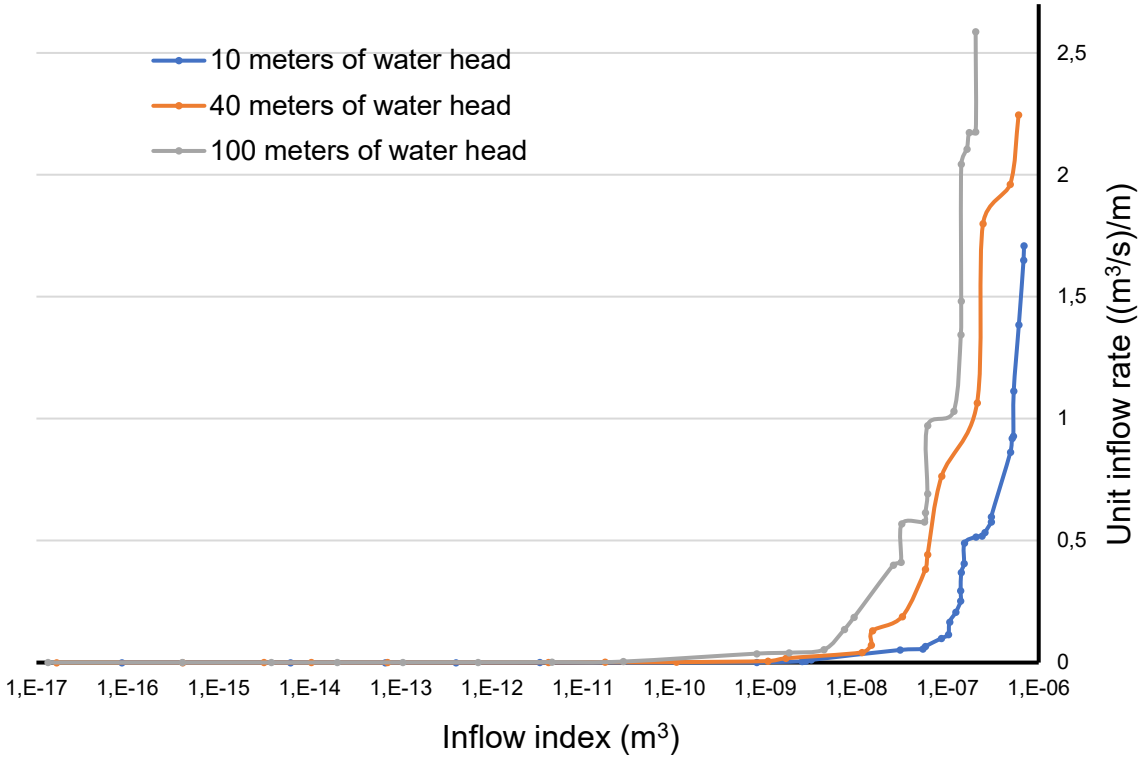

Fig 5. The relationship between the inflow index and inflow rate to the tunnel for the cases of the rock mass that are listed in Table 2. The inflow index is calculated using Eq.(11)

As depicted in Fig 5, a discernible relationship emerges between the inflow rate to the tunnel and the inflow index. Notably, the inflow rate exhibits a direct correlation with the increasing values of the inflow index. On a separate note, when the inflow index is held constant, a distinct trend emerges: the unit inflow rate to the tunnel experiences a rise with an increase in the water head. Furthermore, it is essential to highlight that, within a consistent level of hydraulic head above the tunnel, the inflow index stands as the sole determinant governing the inflow rate to the tunnel. This underscores the pivotal role played by the inflow index in influencing the hydraulic behavior within the tunnel, emphasizing its significance in predicting and understanding the associated inflow

dynamics. The intricate interplay between the inflow index, water head, and hydraulic head above the tunnel unfolds a nuanced understanding of the factors influencing tunnel inflow, contributing to a more comprehensive characterization of the system's hydraulic response.

3 Discussion

Developing and introducing an index that is representative to the inflow rate to the tunnel is not focused by the existing research and can be applicable in underground tunnels that aim to be excavated in a fractured rocky formation below the level of water table. To develop this index, we assumed that the rock mass includes persistent joint sets and tunnel has a circular cross section. As a result, the inflow index for a tunnel could be calculated using Eq.(11) and on this basis, this index depends on the tunnel radius (R), the angle between joint set and tunnel direction (Θ), spacing (S), and the hydraulic aperture (b). However, the impact of parameters on the inflow index, and subsequently on the inflow rate, is not the same. In this regard, Fig 6 has been illustrated for showing the effect of each parameter on inflow index.

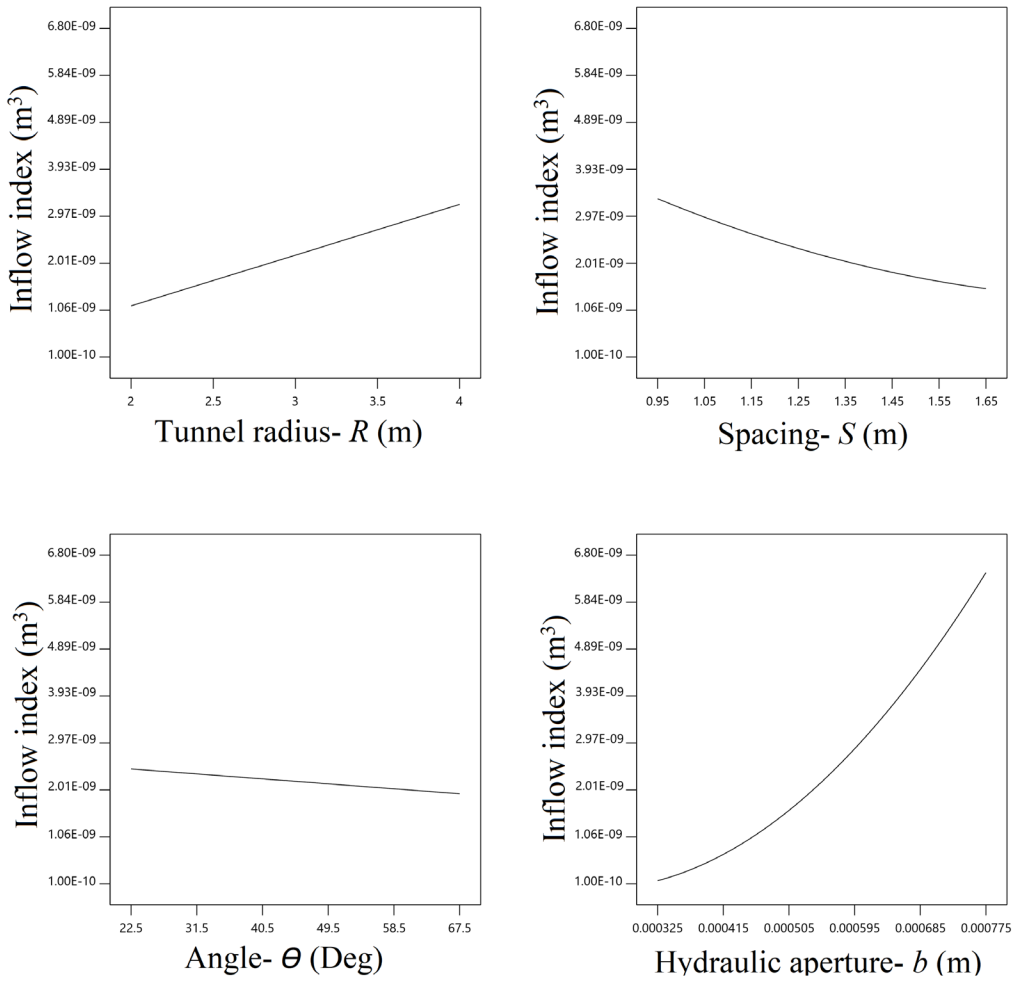

Fig 6. The impact of effective parameters on the inflow index

As depicted in Fig 6, the hydraulic aperture has the greatest and the angle Θ has the lowest impact on the inflow index. In this regard, by increasing the tunnel radius and decreasing the joint spacings, the inflow index increases, accordingly.

Fig 5, shows the variation of the tunnel inflow rate by inflow index. As the values of inflow rate in this diagram have been collected by application of a wide range of hydraulic aperture, the diagram may be less realistic compared to the actual values of inflow rate. To study more real range of the inflow rate and consequently, relevant range of the inflow index, the diagram of Fig 5 is magnified in lesser values of the inflow rate to the tunnel and the relevant section has been illustrated in Fig

7. It is essential to highlight that the inflow index increases with the expansion of the tunnel radius, a relationship demonstrated in Fig 6 and substantiated by the Eq. (11).

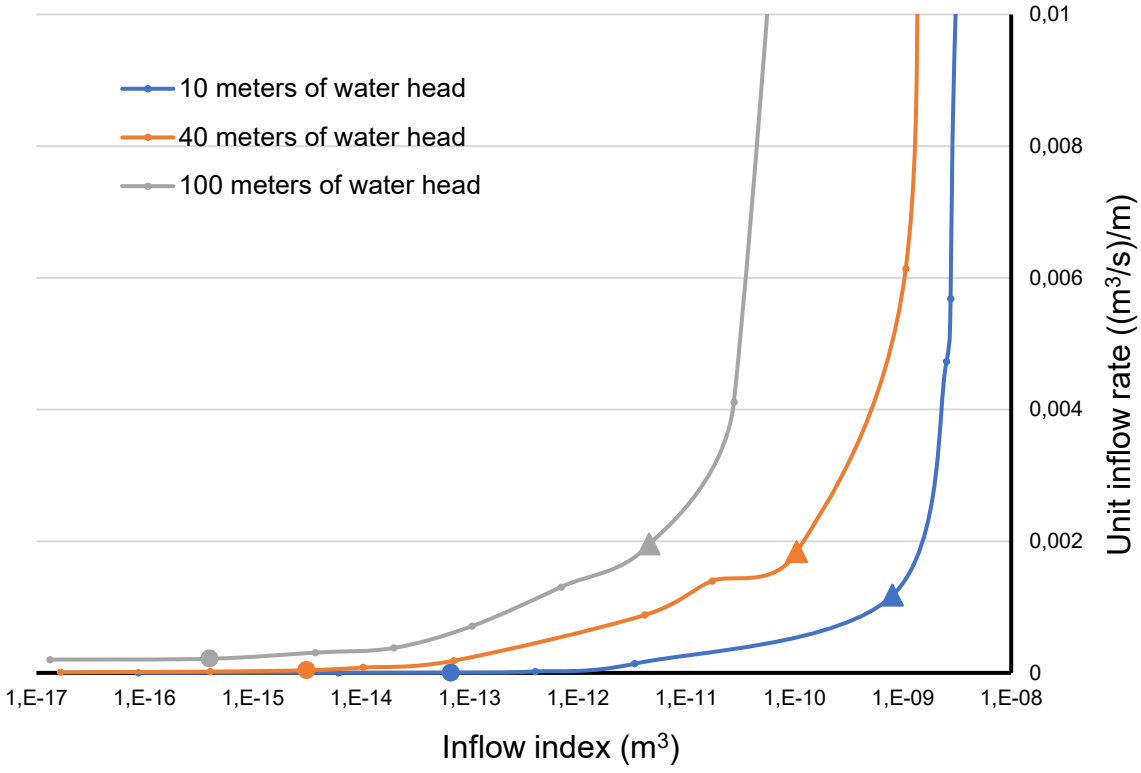

Fig 7. The magnified section of Fig 5 relating to the lower values of the inflow rate and inflow index

Based on Fig 7, same as Fig 5, in the lesser values of the inflow rate and inflow index, by increasing the inflow index, the inflow rate increases, accordingly. However, there are three phases that exist in these diagrams, low, medium, and high inflow rate. The section of the diagram that is placed before the circle point in Fig 7, is the low inflow phase. In this section, the inflow rate doesn't change effectively by increasing the inflow index. The medium inflow rate is placed between the circle point and triangle point (or rapid rising point). In this section, the inflow rate gradually increases by increasing the inflow index. After triangle point, a rapid increase of inflow rate by inflow index occurs. From Fig 7 it could be concluded that the inflow rate to the tunnel could be classified based on the inflow index and level of the water head.

As depicted in Fig 7, the inflow rate-inflow index diagram moves up and to the left by increasing the water head. As a result, the rapid rising point (triangle point in Fig 7) and circle points are moved to the same direction, as well. It means that by increasing the water head, the water inrush phase will begin in the lower inflow indexes and higher values of the inflow rate.

Fig 8 shows the variation of the inflow rate by inflow index and water head. The curved lines show the isolines of the inflow rate to the tunnel and as a result, the value of the inflow rate between each pair of isolines is limited to the marked values of inflow rate for each line. On this basis and by knowing the inflow index and water height above the tunnel, the inflow rate can be classified according to the selected criteria for the values of inflow rate. For example, level 1 in Fig 8 shows the permissible limits for water head and inflow index to obtain the inflow rate less than 2×10^{-4} $((m^3/s)/m)$ and level 2 is limited between 2×10^{-4} and 2×10^{-2}.

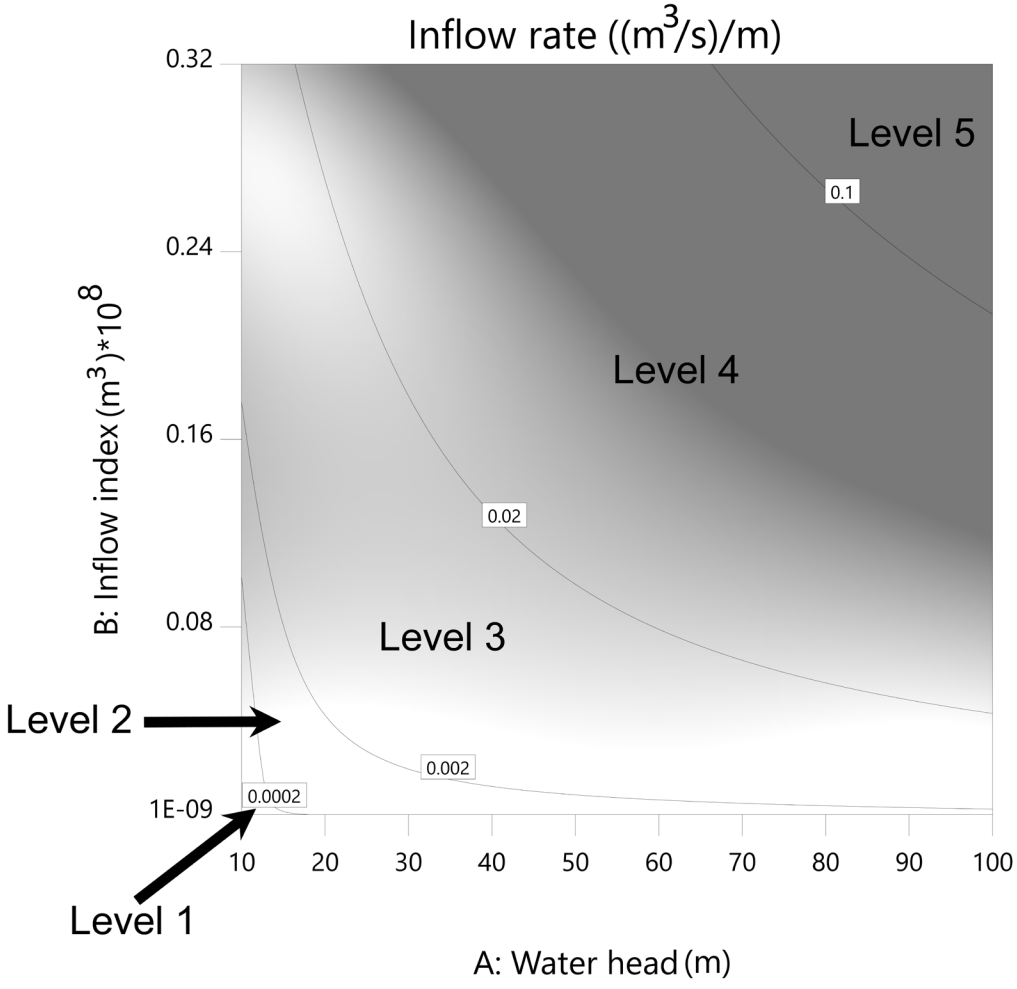

235

236 *Fig 8. Classification of the inflow rate to the tunnel as a function of inflow index and water head above the tunnel*

237 Despite selection of the values of the inflow rate in this article are performed only for showing the
238 possible means of classification of the inflow rate to the tunnel by inflow index and water head
239 above the tunnel, field data can be used for developing a more practical classification of the inflow
240 rate. In this regard, the classification that was introduced by Sharifzadeh (Sharifzadeh, Javadi et al.
241 2012) has been used in this article for defining the inflow index and water head pertinent to each
242 class of inflow rate, according to Table 3.

Table 3. Classification of the inflow rate to the tunnel according to Sharifzadeh (Sharifzadeh, Javadi et al. 2012)

	Inflow ((L/min) /m)		Inflow ((m^3/s) /m)		Description	Flow Mechanism
	Min	Max	Min	Max		
I	0	12.5	0	0.0002	Very Low	Dripping
II	12.5	35	0.0002	0.0006	Low	Leakage
III	35	150	0.0006	0.0025	Medium	Inflow
IV	150	350	0.0025	0.0058	High	High Inflow
V	350	1000	0.0058	0.017	Very High	Inrush
VI	1000	…	0.017	…	Extremely High	Water Burst

For this purpose, the isolines of inflow rate relating to each class of Table 3 have been drawn in Fig 9. According to this figure, by increasing the inflow index and water head, the inflow rate to the tunnel changes from very low to extremely high inflow rate. Furthermore, the impact of inflow index on the inflow rate is more important than the water head, as by a small variation of the inflow index, the inflow mode will be changed. However, based on the classification of the inflow rate to the tunnel, the actual inflow index for a tunnel is mostly less than 6×10^{-10}, as occurrence of extremely high inflow rate is a rare phenomenon when a water head less than 70 meters is existing above the tunnel.

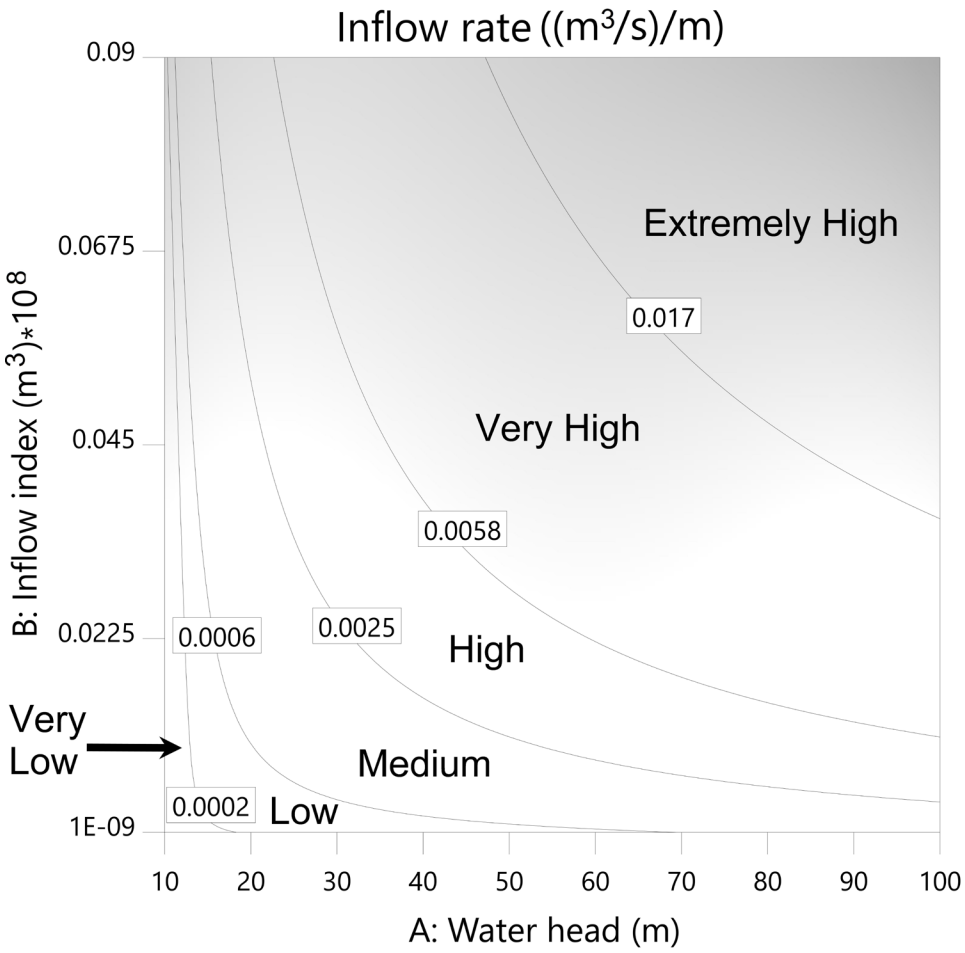

252

253 *Fig 9. Classification of the inflow rate to the tunnel according to Sharifzadeh (Sharifzadeh, Javadi et al. 2012)*

254 *and the relevant inflow index and water head*

255 Drawing from the existing literature (Farhadian and Nikvar-Hassani 2019), numerous analytical
256 techniques have been formulated to compute the rate of water inflow into tunnels. Analytical
257 equations designed to predict water seepage into joined underground tunnels are traditionally
258 designed for application in homogeneous and isotropic geological formations. Nevertheless, it is
259 common for these equations to demonstrate a tendency to overestimate the inflow rate, especially
260 when they are employed in fractured and discontinuous rock formations. The evaluation of the
261 accuracy of the prediction of the inflow rate inside the tunnel, using the inflow index and the water
262 head above the tunnel, included a comparison with the analytical model developed by El Tani. This

choice was made because El Tani's equation has been used and criticized more compared to other models (El Tani 1999), as illustrated in Eq. (12).

$$Q = 2\pi Kh \frac{1 - 3\left(\frac{r}{2h}\right)^2}{\left[1 - \left(\frac{r}{2h}\right)^2\right] \ln\frac{2h}{r} - \left(\frac{r}{2h}\right)^2} \quad (12)$$

Where K is the equivalent hydraulic conductivity of the rock mass (m/s), r is the tunnel radius (m) and h is the tunnel depth below the water table (m). To calculate the equivalent hydraulic conductivity of a fractured rock mass, the following steps are taken:

a) Determine the Hydraulic Conductivity Matrix for Each Joint Set.
b) Calculate the Total Hydraulic Conductivity Matrix of the rock mass by summing the individual hydraulic conductivities of all joint sets.
c) Obtain the Diagonal Matrix of Hydraulic Conductivity from the Total Hydraulic Conductivity Matrix.
d) Calculate the Equivalent Hydraulic Conductivity by taking the cube root of the product of the three principal hydraulic conductivities, each of which corresponds to an element of the diagonal hydraulic conductivity matrix.

For the purpose of comparison of predicted inflow rates, according to Table 4, three cases of rock mass, each of which consists of three sets of joints, are considered and in each of them a circular tunnel is excavated, so that the water table level is above the tunnel.

Table 4. Inflow rate (Q) according to El Tani's equation (Eq.(12)) and Inflow index for three cases of rock mass each having three joint sets and a circular tunnel has been excavated.

Case No	JS No.	Dip	DD	Spacing (m)	Aperture (m)	Tunnel radius (m)	Inflow index (m^3)	K_{eq} (m/s)	Water head (m)	Q per El Tani (El Tani 1999)

1	**1**	70	140	3	0.0001	2	5.85E-09	0.000496492	90	0.28076853
	2	40	230	0.4	0.0007					
	3	20	390	2	0.00001					
2	**1**	60	36	1.5	0.00003	3	1.50E-11	2.50E-06	60	0.000941364
	2	70	95	0.3	0.00007					
	3	33	200	0.1	0.00001					
3	**1**	20	100	2	0.00004	4	1.03E-12	1.54E-06	50	0.000484181
	2	20	270	1	0.00003					
	3	70	30	3	0.000001					

The inflow rate to the tunnel in case numbers 1 to 3 of Table 4 has been determined by using the relevant inflow index and water head above the tunnel. For this purpose, Fig 9 has been used and the pertinent inflow rate for each case has been illustrated in Fig 10.

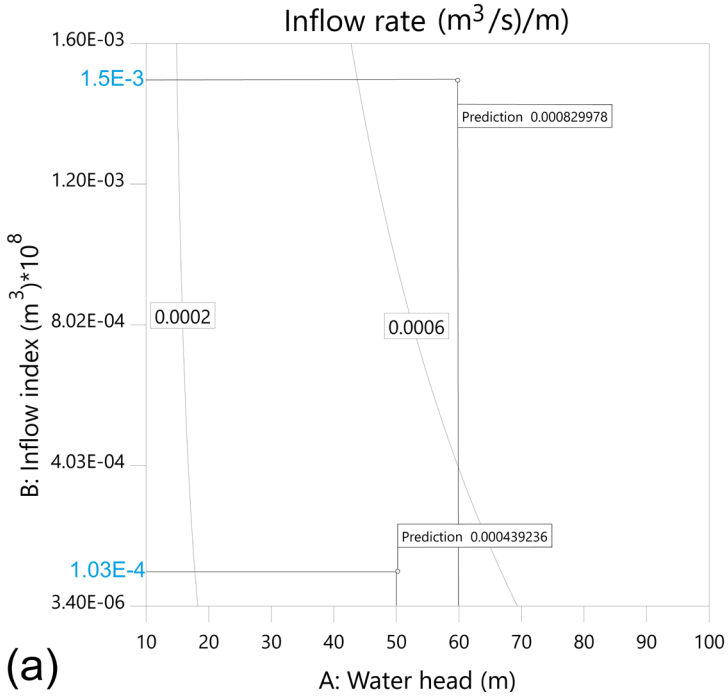

284

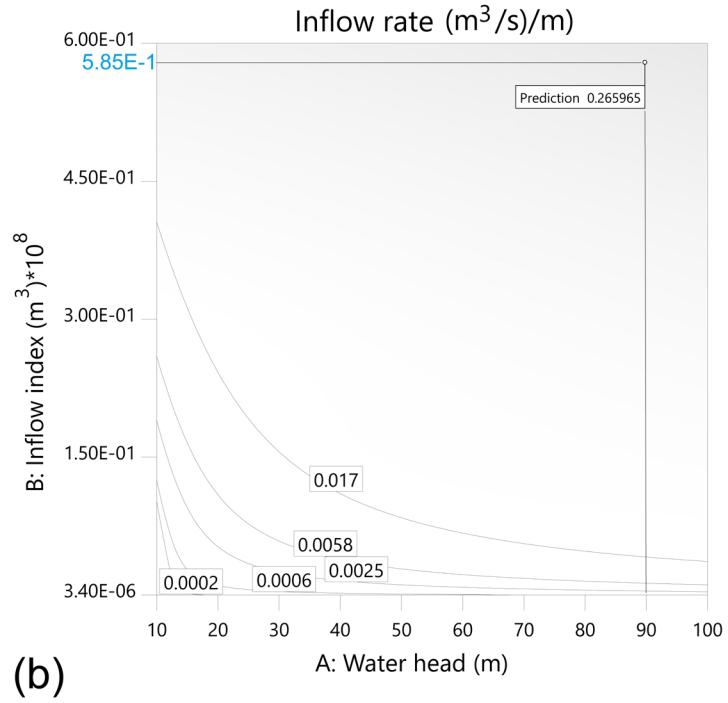

285

286 *Fig 10. Calculation of the inflow rate to the tunnel for three cases of the rock mass in Table 4 by using the inflow index.*

287 *(a) cases 2&3 and (b) case 1 of Table 4.*

288 According to Fig 10 and Table 4, the calculated inflow rate by using inflow index is in a good
289 agreement with the analytical model that was developed by El Tani. On this basis, Fig 10a shows
290 two cases of the tunnel that their inflow rate is medium (for water head equal to 60m) and low (if
291 water head is 50m). In addition, Fig 10b illustrates a case that the inflow rate is Extremely high,
292 according to the classification of inflow rate proposed by Sharifzadeh (Sharifzadeh, Javadi et al.
293 2012). In addition to the good agreement between calculating the input flow rate using the El Tani
294 equation (Eq.(12)) and the flow index (Fig 9), the inflow rate values are such that a wide range of
295 classifications are covered., i.e., from extremely high to low inflow rate, and it shows the
296 comprehensiveness of the proposed index, that is the inflow index, for prediction of the inflow rate
297 to the tunnel.

298 To develop the analytical model for calculation of the inflow index according to Eq.(11), we
299 assumed that the rock mass includes persistent joint sets, the hydraulic aperture is fixed for all
300 fractures in a joint set, the fractures are fully connected, and the tunnel has circular cross section.
301 As a result of these simplifying assumptions, there will be limitations to the application of this
302 model to real rock and tunnel cases, each of which is related to a simplifying assumption. Despite
303 these limitations, the inflow index remains a measurable parameter by considering modifications
304 that can be applied to Eq.(11) for each of these limitations. For example, if the joint sets were not
305 fully persistent, a coefficient for the case of nonpersistent joint sets can be developed and added to
306 Eq. (11). For any deviation from the simplifying assumptions of Eq. (11), e.g., lack of connectivity,
307 joint infillings, etc., a specific coefficient can be developed to increase the applicability of this
308 equation for the real cases of rock mass and tunnel.

309 On the other hand, the inflow index can also be used in fieldwork. Eq.(11) calculates the product
310 of the length of fracture traces at the wall of the tunnel and the square of the corresponding aperture,
311 which is a parameter that can be measured by surveying of the discontinuities. In addition,

observation wells at ground level can be used to determine the water table and, accordingly, determine the water head above the tunnel. As a result, by accessing this data, tunnel engineers and practitioners can estimate the expected inflow to the tunnel during tunnel excavation.

4 Summary and conclusion

In this article, an analytical model has been developed for defining an index that could be used as a representative to the inflow rate to the tunnel, according to Eq.(11). To use this model, the tunnel direction and radius, hydraulic aperture, dip & dip direction of joint sets, and joint spacings have to be identified. The inflow index is shown to increase by hydraulic aperture and tunnel radius, and decreases by spacing and the angle between tunnel and normal to joint sets. Among all parameters, the impact of hydraulic aperture is more important than the others, as the inflow index increases rapidly by a slight increase of the hydraulic aperture.

The increase in the inflow index is shown to correspond to an increase in the inflow rate, and the relevant diagram is moved up and left by increasing the water head. Three steps have been observed in the inflow rate-inflow index diagram in a constant level of water head, as low, medium and high (inrush) inflow rates. Furthermore, a specific point exists in all diagrams that the mode of inflow to the tunnel changes from medium to high inflow rates. Being aware of this threshold and related inflow index will be helpful for the practitioners and tunneling engineers to judge about the probable state of inflow rate to the tunnel by knowing the effective parameters, according to Eq.(11).

Based on the existing classification for the amount of inflow rate to the tunnel, inflow index and water head can be used for prediction of the level of inflow rate and also, for each class of inflow rate, a relevant range for inflow index and water head can be specified. However, as a general rule, the inflow rate increases by increasing the inflow index and water head and in this regard, the inflow

index has a significant impact on the inflow rate and can be considered as an efficient representative for evaluation of the inflow rate to the tunnel.

CRediT authorship contribution

Alireza Shahbazi: Conceptualization, Resources, Data curation, Software, validation, Methodology, Writing-original draft; Ali Saeidi: Conceptualization, Supervision, Investigation, Methodology, Project administration, Writing-review & editing; Romain Chesnaux: Supervision, Writing-review & editing; Alain Rouleau: Conceptualization, Supervision, Writing-review & editing

Declaration of competing interest

The authors declare that there is no conflict of interest associated with this publication.

Acknowledgments

The authors would like to thank the Itasca Consulting Group in Minneapolis for the IEP Research Program, especially Jim Hazzard, for his valuable technical help and advice.

References

Darcy, H. (1856). Les fontaines publiques de la ville de Dijon: exposition et application, Victor Dalmont.

El Tani, M. (1999). Water inflow into tunnels. Proceedings of the World Tunnel Congress ITA-AITES. Switzerland, International Tunneling and Underground Space Association**:** 61–70.

Farhadian, H., A. N. Hassani and H. Katibeh (2017). "Groundwater inflow assessment to Karaj Water Conveyance tunnel, northern Iran." KSCE Journal of Civil Engineering **21**(6): 2429-2438.DOI: https://doi.org/10.1007/s12205-016-0995-2.

Farhadian, H. and A. Nikvar-Hassani (2019). "Water flow into tunnels in discontinuous rock: a short critical review of the analytical solution of the art." Bulletin of Engineering Geology and the Environment **78**(5): 3833-3849.DOI: https://www.doi.org/10.1007/s10064-018-1348-9.

Frenelus, W., H. Peng and J. Zhang (2021). "Long-term degradation, damage and fracture in deep rock tunnels: A review on the effect of excavation methods." Frattura ed Integrità Strutturale **15**(58): 128-150.DOI: https://doi.org/10.3221/IGF-ESIS.58.10.

Herbert, A., J. Gale, R. MacLeod and G. Lanyon (1991). Modelling for the Stripa site characterization and validation drift inflow: prediction of flow through fractured rock. Sweden**:** 315.

Hudson, J. A., J. W. Cosgrove, K. Kemppainen and E. Johansson (2011). "Faults in crystalline rock and the estimation of their mechanical properties at the Olkiluoto site, western Finland." Engineering Geology **117**(3): 246-258.DOI: https://doi.org/10.1016/j.enggeo.2010.11.004.

Itasca Consulting Group, I. (2021). 3DEC — Three-Dimensional Distinct Element Code. Minneapolis, Itasca. **135**.

Lv, Y., Y. Jiang, W. Hu, M. Cao and Y. Mao (2020). "A review of the effects of tunnel excavation on the hydrology, ecology, and environment in karst areas: Current status, challenges, and perspectives." Journal of Hydrology **586**: 124891.DOI: https://doi.org/10.1016/j.jhydrol.2020.124891.

Shadabfar, M., M. Mahsuli, Y. Zhang, Y. Xue and H. Huang (2022). "Probabilistic data-driven framework for performance assessment of retaining walls against rockfalls." Probabilistic Engineering Mechanics **70**: 103339.DOI: https://doi.org/10.1016/j.probengmech.2022.103339.

Shahbazi, A., R. Chesnaux and A. Saeidi (2021). "A new combined analytical-numerical method for evaluating the inflow rate into a tunnel excavated in a fractured rock mass." Engineering Geology **283**: 106003.DOI: https://doi.org/10.1016/j.enggeo.2021.106003.

Shahbazi, A., A. Saeidi and R. Chesnaux (2020). "A review of existing methods used to evaluate the hydraulic conductivity of a fractured rock mass." Engineering Geology **265**: 105438.DOI: https://doi.org/10.1016/j.enggeo.2019.105438.

Shahbazi, A., A. Saeidi, R. Chesnaux and A. Rouleau (2021). "The Specific Length of an Underground Tunnel and the Effects of Rock Block Characteristics on the Inflow Rate." Geosciences **11**(12).DOI: https://doi.org/10.3390/geosciences11120517.

Shahbazi, A., A. Saeidi, R. Chesnaux and A. Rouleau (2023). "Effects of fracture-system geometrical parameters on the inflow rate into a tunnel in rock: a numerical modelling experiment." Quarterly Journal of Engineering Geology and Hydrogeology **56**(2): qjegh2021-2128.DOI: doi:10.1144/qjegh2021-128.

Sharifzadeh, M., M. Javadi and H. Zarei (2012). The Role of Geological Structures to Tunnel Inflow, Modelling Strategies and Predictions. World Tunnel Congress, Bangkok, Thailand.

Witherspoon, P. A., J. S. Y. Wang, K. Iwail and J. E. Gale (1979). "Validity of cubic law for fluid flow in a deformable rock fracture." Water Resources Research **16**(6): 1016-1024.DOI: https://doi.org/10.1029/WR016i006p01016.